Post-Synthetic Modification of a Metal–Organic Framework Glass

Alice M. Bumstead[†], Ignas Pakamorė[‡], Kieran D. Richards[†], Michael F. Thorne[†], Sophia S. Boyadjieva[‡], Celia Castillo-Blas[†], Lauren N. McHugh[†], Adam F. Sapnik[†], Dean S. Keeble[§], David A. Keen[‖], Rachel C. Evans[†], Ross S. Forgan[‡], and Thomas D. Bennett[†*]

[†] Department of Materials Science and Metallurgy, University of Cambridge, Cambridge, CB3 0FS, UK.

[‡] WestCHEM, School of Chemistry, The University of Glasgow, University Avenue, Glasgow, G12 8QQ, UK.

[§] Diamond Light Source Ltd, Diamond House, Harwell Campus, Didcot, Oxfordshire, OX11 0DE, UK.

[‖] ISIS Facility, Rutherford Appleton Laboratory, Harwell Campus, Didcot, Oxfordshire, OX11 0QX, UK.

* Email: tdb35@cam.ac.uk

ABSTRACT: Melt-quenched metal–organic framework (MOF) glasses have gained significant interest as the first new category of glass reported in 50 years. In this work, an amine-functionalized zeolitic imidazolate framework (ZIF), denoted ZIF-UC-6, was prepared and demonstrated to undergo both melting and glass formation. The presence of an amine group resulted in a lower melting temperature compared to other ZIFs, whilst also allowing material properties to be tuned by post-synthetic modification. As a prototypical example, the ZIF glass surface was functionalized with octyl isocyanate, changing its behavior from hydrophilic to hydrophobic. Post-synthetic modification therefore provides a promising strategy for tuning the surface properties of MOF glasses.

INTRODUCTION

There is growing interest in the field of metal–organic frameworks (MOFs) towards material properties such as framework flexibility and stimuli induced structural transitions.[1–3] Such transformations can be induced by chemical inclusion such as gas sorption, or, by physical stimuli including pressure, temperature or UV light.[3,4] It has recently been observed that temperature can induce a solid-liquid transition *i.e.*, melting, in several MOFs.[5,6] Cooling of these liquids can yield melt-quenched glasses, which retain the local metal-ligand connectivity of the parent crystalline framework, though lack any long range periodicity.[7] These melt-quenched glasses retain some porosity in the glass phase, and, as they pass through a liquid state, can be more easily processed compared to typical crystalline powders.[6]

Melting and glass formation in MOFs are most commonly observed in zeolitic imidazolate frameworks (ZIFs), a subset composed of tetrahedral metal ions coordinated to imidazolate (Im – $C_3H_3N_2^-$) type linkers.[7–9] Melting in ZIFs has been demonstrated computationally to be a dynamic process occurring on a picosecond timescale; de-coordination of an imidazolate linker is rapidly followed by re-coordination of a new linker in its place.[6] The reversible transition when a liquid is frozen as an amorphous solid, *i.e.* without crystallization, is known as the glass transition (occurring at temperature T_g).[7,10]

A reduction of the melting temperature (T_m) and T_g of ZIFs would facilitate large-scale material processing at lower temperatures, improve the optical quality of the glasses and prevent decomposition related discoloration.[11–13] Strategies designed to reduce T_m in ZIFs typically involve changing the chemical functionality of the crystalline framework either at the metal center, such as by replacing the more usual Zn^{2+} with Co^{2+}, or at the organic linker, by using various mixed-linker approaches.[11,12] Highly disordered systems such as $[Co_{0.2}Zn_{0.8}(Im)_{1.95}(bIm)_{0.025}(ClbIm)_{0.025}]$ (bIm – benzimidazolate – $C_7H_5N_2^-$, ClbIm – 5-chlorobenzimidazolate – $C_7H_4N_2Cl^-$) have been found to exhibit melting temperatures of *ca.* 310 °C, *i.e.*, amongst the lowest currently known for ZIFs.[10] The use of electron-withdrawing linkers to lower both T_m and T_g by weakening the Zn-N coordination bond has also been reported.[14,15] For example, the ClbIm linker in ZIF-UC-5 $[Zn(Im)_{1.8}(ClbIm)_{0.2}]$ resulted in a lower T_m (428 °C) and T_g (336 °C) compared to a non-halogenated structural isomorph $[Zn(Im)_{1.8}(mbIm)_{0.2}]$ (mbIm – 5-methylbenzimidazolate – $C_8H_7N_2^-$) (T_m = 440 °C, T_g = 350 °C).[14]

Amine functionalized ZIF glasses are interesting due to their potential adsorption capability for Lewis acidic gases such as CO_2,[16–18] the hydrophilic nature imparted to the glasses by the amine moiety, and the possibility for post-synthetic modification (PSM) of the ZIF glass to further tune its properties.[19–21] Given these advantages, it is surprising that there have only been a few reports of amine functionalized crystalline ZIFs,[16,17] and, no reports of any ZIF glasses containing this functionality.[22–24]

Currently, the chemical functionality available within ZIF glasses remains limited.[14,15] In the inorganic glass domain, chemical modification is achieved through, for example, post-synthetic ion exchange of Na^+ ions in sodium silicate glasses for larger K^+ ions. This is used to strengthen the glass surface, resulting in toughened glasses, suitable for smartphone screens.[25,26] Other methods include ion implantation, where the glass surface is bombarded with high energy ions, altering the surface chemistry and hence optical and mechanical properties, such as refractive index and material hardness.[27,28] Inorganic glasses have also been modified with polymer coatings to enhance both the hydrophobicity and durability of the glass surface.[29,30] PSM is also used to produce porous inorganic glass, *e.g.* Vycor® glass (Corning Incorporated), which is prepared by post-synthetic treatment of a melt-quenched inorganic glass with acid to remove the boron and alkali metal rich components.[31,32]

PSM of crystalline MOFs has also been demonstrated, utilizing reactive chemical functionalities included in the framework.[19–21] For example, the nucleophilic amine functionality on 2-aminoterephthalic acid in IRMOF-3 has been reacted with acetic anhydride, resulting in an amide functionalized framework.[33] Further studies demonstrated the versatility of amine functionalities for reacting with various electrophiles including carboxylic acids, acid anhydrides and isocyanates.[34–36] Despite this, PSM has not been demonstrated on melt-quenched MOF glasses or indeed on any non-crystalline MOF system. This raises two questions: is it achievable, and if it is what effect would PSM have on the physical and chemical properties of the glass?

Here, we synthesize a previously unknown amine-functionalized ZIF, denoted ZIF-UC-6, possessing the **cag** network topology (**Fig. 1**). We first demonstrate its liquid and glass forming behavior, before utilizing the amine functionality to investigate PSM on both crystalline ZIF-UC-6 and its glass, denoted a_gZIF-UC-6. This allowed us to investigate the effect of PSM on the physical properties of a ZIF glass for the first time.

RESULTS AND DISCUSSION

Crystalline ZIF-UC-6. Single crystals of ZIF-UC-6 were grown by solvothermal synthesis (**Methods**). Specifically, zinc nitrate hexahydrate (0.32 mmol), imidazole (6.76 mmol) and 5-aminobenzimidazole (abIm, 0.75 mmol) were dissolved in *N*,*N*-dimethylformamide (DMF), yielding a dark red solution which was heated to 130 °C and held there for 48 hr (**Figs. S1**, **S2**). Slow cooling of the reaction mixture at 5 °C hr^{-1} resulted in burgundy single crystals (**Fig. S3**). Single crystal X-ray diffraction (SCXRD) confirmed their crystallization in the *Pbca* space group (a = 15.839(2) Å, b = 15.599(2) Å, c = 17.984(2) Å, V = 4443.3(9) $Å^3$) (**Fig. 1, Fig. S4, Table S1**). ZIF-UC-6 crystallizes with a unit cell very similar to that of the prototypical glass-former ZIF-62 $[Zn(Im)_{2-x}(bIm)_x]$.[11,37] The abIm ligand is localized on one of the four possible linker positions; a 0.4:0.6 abIm:Im occupancy ratio on this site leads to an overall composition of $[Zn(Im)_{1.82}(abIm)_{0.18}]$ for this particular crystal. A phase pure burgundy microcrystalline powder sample was then synthesized (**Methods**, **Figs. S5-S7, Table S2**) with a composition of $[Zn(Im)_{2-x}(abIm)_x]$ (where x = 0.18) confirmed by ^{1}H NMR spectroscopy (**Fig. S8**), correlating closely to the single crystal structure which can be taken as representative of the bulk polycrystalline powder.

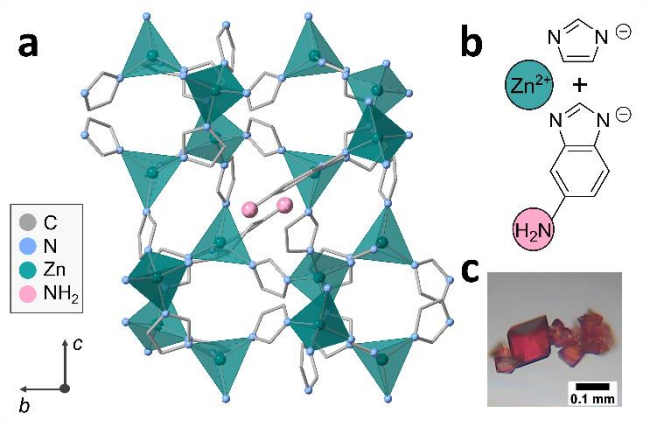

Figure 1. (a) Crystal structure of ZIF-UC-6, *Pbca* space group, **cag** topology, viewed down the *a* unit cell axis. Atoms shown are carbon (grey), nitrogen (blue) and zinc (green). ZnN_4 tetrahedra have been highlighted in green, amine groups have been highlighted in pink, whilst hydrogen atoms have been omitted for clarity. Disorder resulting from multiple linker occupancy has also been omitted for clarity. (b) Zn^{2+} ion alongside imidazolate and aminobenzimidazolate linkers in ZIF-UC-6. (c) Optical image of dark burgundy single crystals of ZIF-UC-6.

Thermal Behavior and Glass Formation. The thermal response of ZIF-UC-6 was studied using differential scanning calorimetry (DSC) and thermogravimetric analysis (TGA) (**Fig. 2**, **Fig. S9-S11**). A 3.5% mass loss occurred below 220 °C and was accompanied by a broad endotherm in the DSC with a peak at 211 °C. This is ascribed to residual solvent in the pores after activation in line with previous studies.[13] Above 507 °C, significant sample decomposition began as indicated by a sharp drop in mass (**Fig. S9**). Below this temperature, a melting endotherm was observed in the DSC (T_m = 345 °C) (**Fig. 2, Fig. S11**). A 1.8% mass loss occurred between desolvation and 400 °C, suggesting that melting is accompanied by trace levels of decomposition (**Fig. S10**). Reheating this sample gave a T_g = 316 °C (**Fig. 2, Fig. S11**). Samples of ZIF-UC-6 heated above 400 °C and subsequently cooled will henceforth be denoted a_gZIF-UC-6 to highlight their transformation to the glass phase.

ZIF-UC-6 melts at a markedly lower temperature than other isostructural – *Pbca* space group, **cag** topology – melting ZIFs with different functionalized linkers such as TIF-4 $[Zn(Im)_{1.8}(mbIm)_{0.2}]$ (mbIm – 5-methylbenzimidazolate – $C_8H_7N_2$) (T_m = 440 °C) and ZIF-UC-5 $[Zn(Im)_{1.8}(ClbIm)_{0.2}]$ (ClbIm – 5-chlorobenzimidazolate – $C_7H_4N_2Cl^-$) (T_m = 428 °C).[14] A recent study highlighted that T_m has both an enthalpic contribution (ΔH_{fus}) and an entropic contribution (ΔS_{fus}), and that lowering ΔH_{fus} and increasing ΔS_{fus} both result in a reduction of T_m.[38] We applied their methodology here and compared the enthalpic and entropic contributions to melting in ZIF-UC-6 to those reported for TIF-4 and ZIF-UC-5 (**Table S3, Fig. S12**).[14] ZIF-UC-6 had the lowest ΔH_{fus} and ΔS_{fus} of the three ZIFs compared. Additionally, both ΔH_{fus} and ΔS_{fus} increased from ZIF-UC-6 to ZIF-UC-5 to TIF-4, following the same trend as T_m. This implies that the major contribution to T_m is ΔH_{fus}, and that the low T_m of ZIF-UC-6 results from weaker Zn-N coordination bonds.

The amine functionality in ZIF-UC-6 also has the potential to undergo hydrogen bonding. Therefore, one possible explanation for the low T_m of ZIF-UC-6 is that dynamic movement of the framework during melting may result in the potential formation of temporary hydrogen bonding interactions. These dispersive interactions may stabilize the uncoordinated linkers that form during the melting process, thus reducing the energy barrier to melting.[6]

The T_g for a_gZIF-UC-6 (T_g = 316 °C) is also lower when compared to these other two ZIF glasses: a_gTIF-4 (T_g = 350 °C) and a_gZIF-UC-5 (T_g = 336 °C). This may also be attributed to the lower ΔH_{fus}, *i.e.*, weaker coordination bonds, in ZIF-UC-6 compared to these frameworks. Additionally, the Van der Waals volume of $-NH_2$ is 10.54 cm^3 mol^{-1}, whilst $-CH_3$ in TIF-4 (13.67 cm^3 mol^{-1}) and -Cl in ZIF-UC-5 (12.0 cm^3 mol^{-1}) are both larger.[39,40] The T_g also depends on steric freedom *i.e.*, how easily molecules can move past one another, so the smaller linker substituent in a_gZIF-UC-6 also likely contributes to its lower T_g.[7,41] The use of amine-functionalized linkers therefore provides a promising strategy for preparing ZIFs with both a lower T_m and T_g.

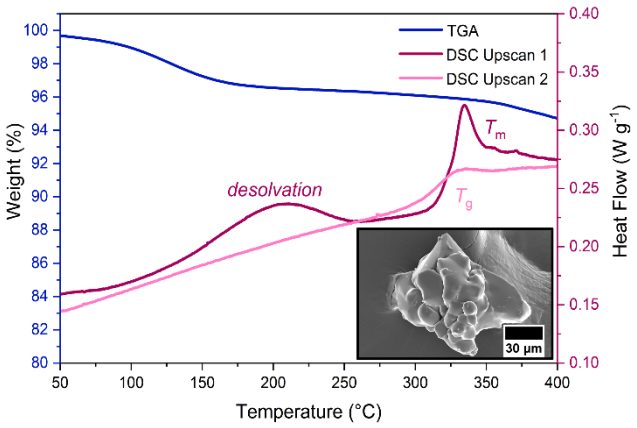

Figure 2. TGA curve (1st upscan – blue) and DSC traces (1st upscan – dark pink; 2nd upscan – light pink) of ZIF-UC-6 in the region of 50-400 °C. The 1st upscan of the DSC exhibits a desolvation endotherm at 211 °C followed by a melting endotherm. T_m was taken as the offset of this endotherm with T_m = 345 °C. The 2nd DSC upscan shows a T_g of 316 °C. Inset shows an SEM image of a_gZIF-UC-6 displaying a loss of crystal facets and evidence of particle coalescence and flow.

A sample of a_gZIF-UC-6 quenched from 400 °C appeared visually to have undergone melting, with evidence of particle coalescence as well as the presence of flow related striations (**Fig. 2 Inset, Fig. S13**). This sample was then confirmed to be X-ray amorphous with a composition identical to the parent crystalline material *i.e.*, $[Zn(Im)_{1.82}(abIm)_{0.18}]$ (**Figs. S5, S14**). The thermal stability of the glass was found to be very similar to the crystalline material (**Fig. S15-S16**).

CO_2 gas sorption on both crystalline ZIF-UC-6 and a_gZIF-UC-6 revealed significant differences. ZIF-UC-6 exhibited a CO_2 uptake of 46.9 cm^3 g^{-1} at standard temperature and pressure (STP) (**Fig. 3, Fig. S17, Table S4**), with this value being comparable to some of the highest values reported for CO_2 uptake in ZIFs.[15,23,42] Meanwhile a_gZIF-UC-6 displayed a lower CO_2 uptake (23.0 cm^3 g^{-1} at STP) as well as more pronounced hysteresis, as expected due to the collapse of the crystalline framework upon glass formation (**Fig. 3, Fig. S18, Table S5**).

To further investigate the structures of ZIF-UC-6 and a_gZIF-UC-6, X-ray total scattering data were collected at the Diamond Light Source, beamline I15-1 (**Methods, Fig. S19**). Fourier transformation of the corrected total scattering data gave the pair distribution function which we have presented here in the $D(r)$ form (**Fig. 4**). Short-range order correlations of ZIF-UC-6 (labelled 1-5) were maintained in a_gZIF-UC-6 with little variation in the intensities of these peaks, implying that chemical connectivity is largely retained in the glass phase. However, long-range order (> 8.0 Å) was lost in a_gZIF-UC-6, supporting the lack of long-range periodicity in the glass phase (**Fig. 4**).

Post-Synthetic Modification of a_gZIF-UC-6. The use of PSM to further tune the properties of a MOF glass has yet to be reported, despite the potential to alter its thermal and surface properties. PSM of crystalline MOFs has already been studied in considerable depth[19,43] with the use of amine-functionalized linkers being a common choice as the site for further reaction.[34–36] The amine functionality on the abIm linker in both ZIF-UC-6 and a_gZIF-UC-6 therefore provides a promising target for further modification with various electrophiles.

Anhydrides are frequently used for PSM of amine-functionalized MOFs as they are highly reactive electrophiles, resulting in amide-functionalized frameworks alongside a carboxylic acid by-product.[19,34] However, although ZIFs are well known for their thermal and chemical stability, their susceptibility to acid digestion is well reported.[8,44] As such, an alternative electrophile was needed for ZIF-UC-6. Isocyanates are also reported to react with amine functionalized frameworks, yielding urea functionalities and no by-products (**Fig. S20**).[35,36] These reasons, in addition to the desire to ultimately alter the surface hydrophobicity of the glass, led to octyl isocyanate being selected as the modification reagent, as it combined both an electrophilic functionality with a hydrophobic carbon tail (**Fig. S21**).

The low amine content in ZIF-UC-6 meant only 9% of the linkers contained the reactive amine group necessary for PSM. Furthermore, the small pore size within ZIF-UC-6 (< 6 Å) meant only surface modification would be possible, as octyl isocyanate (*ca.* 13 Å) (**Fig. S22**) would be too large to enter the pores of the framework.[45] This provided an additional challenge compared to previous studies which have generally focused on materials where all of the linkers were accessible for PSM.[19,34]

There appeared to be two possible strategies to prepare a hydrophobic ZIF glass by PSM: (i) perform PSM on crystalline ZIF-UC-6 before melt-quenching, or (ii) prepare the glass first, then perform PSM on the glass surface directly. As PSM has already been reported on crystalline MOFs quite extensively,[19,43] strategy (i) was attempted first.

Preparation of Modified a_gZIF-UC-6 – Strategy (i). The procedure for PSM on crystalline ZIF-UC-6 was based on previous reports on the modification of IRMOF-3.[33,35] Briefly, ZIF-UC-6 was suspended in a dilute solution of octyl isocyanate in chloroform and left to react for 24 hr before a rigorous washing and activation procedure (**Methods**). The retention of crystallinity after PSM was confirmed by powder X-ray diffraction (PXRD), and no crystalline impurities introduced during the PSM process were found (**Fig. S23, Table S6**).

Fourier-transform infrared (FTIR) spectroscopy was performed on unmodified and modified ZIF-UC-6 (**Fig. S24**).

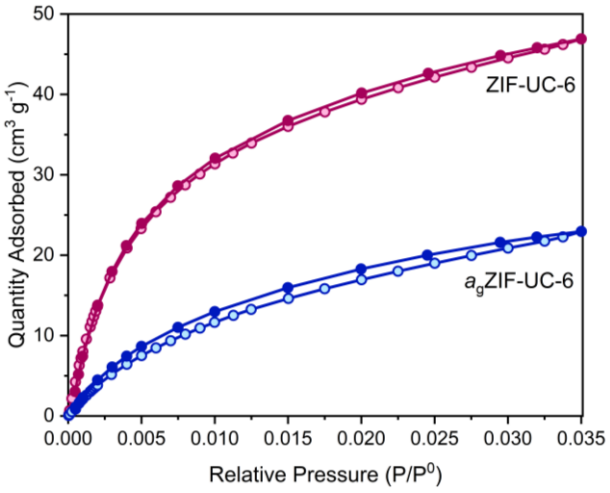

Figure 3. CO_2 gas sorption isotherms for ZIF-UC-6 (pink) and a_gZIF-UC-6 (blue). Adsorption isotherms represented by open circles whilst desorption isotherms represented by closed circles. ZIF-UC-6 had a maximum uptake of 46.9 cm^3 g^{-1} at STP whilst for a_gZIF-UC-6 it was 23.0 cm^3 g^{-1} at STP.

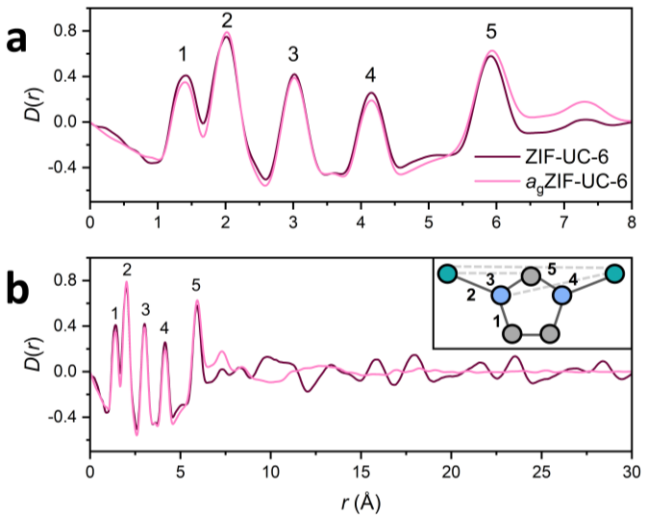

Figure 4. Pair distribution function, $D(r)$, of ZIF-UC-6 (dark pink) and a_gZIF-UC-6 (light pink). (a) Short range order correlations (0-8 Å) undergo minimal changes on glass formation. (b) Full $D(r)$ shows long range order (> 8 Å) is lost after heating. Inset shows molecular connectivity along with some of the key corresponding correlations. The five dominant correlations at low-r are also labelled on the $D(r)$. Atoms shown are carbon (grey), nitrogen (blue) and zinc (green). Hydrogen atoms have been omitted for clarity.

However, no discernible changes in the spectra were observed which is likely due to the low content (9%) of the amine linker. This could also be ascribed to a lack of the amine moiety in the framework, however, the presence of two distinct linker environments by ^{1}H NMR (**Fig. S8**) combined with its strong color and absorbance in the visible spectrum (**Figs. S2, S3, S7**) point to the amine linker being present, albeit at low levels.

^{1}H NMR spectroscopy was performed on the modified sample (**Fig. S25**) along with imidazole, 5-aminobenzimidazole and octyl isocyanate for reference (**Figs. S26-S28**). A new 2 position imidazole singlet peak at 9.53 ppm was observed for modified ZIF-UC-6 that did not correspond to imidazole or 5-aminobenzimidazole and supported the presence of a new imidazole type linker in the structure (**Fig. S25b**). Additionally, multiple new aromatic environments, with matching peak integrations to the new singlet at 9.53 ppm, also supported the formation of a new substituted linker (**Fig. S25c**). Furthermore, clear evidence of the eight-membered carbon chain was also observed below 1.5 ppm, again with peak integrations correlating with the other new environments formed (**Fig. S25d**). The composition of the modified material was then determined by peak integration, giving a formula of $[Zn(Im)_{1.82}(abIm)_{0.16}$(PSM linker)$_{0.02}]$ *i.e.*, an 11% conversion of the available abIm linkers and a 1% conversion of the total organic molecules present within the structure. This conversion was not expected to be discernible by techniques such as CHN microanalysis, as the changes would be within instrumental error. Our experimental observations support this as no significant changes in the wt. % of C, H or N were observed after modification (**Table S7-S8**).

To further support the successful formation of a modified linker, a digested sample of modified ZIF-UC-6 was subjected to high resolution electrospray ionization mass spectrometric analysis. The presence of the molecular ion with formula $[C_{16}H_{24}N_4O]H^+$ (calc: m/z = 289.2028; found: m/z = 289.2023; 1.7 ppm) strongly suggests that covalent modification of 5-aminobenzimidazolate to form the octyl-urea adduct has occurred, rather than physisorption of octyl isocyanate onto the surface of the MOF particles (**Figs. S29, S30**).

To further support that the reactive amine functionality in ZIF-UC-6 was undergoing the PSM reaction and octyl isocyanate was not simply physisorbed on the surface, a control experiment was performed using ZIF-62, as it contains unfunctionalized benzimidazolate linkers. A sample of ZIF-62 $[Zn(Im)_{1.8}(bIm)_{0.2}]$ was prepared by previously reported methods,[46] and reacted with octyl isocyanate in an identical manner to ZIF-UC-6 before being analyzed by ^{1}H NMR (**Fig. S31**). Unlike ZIF-UC-6, there was no evidence for the formation of a new 2 position imidazole proton environment and there was minimal evidence of the carbon chain of octyl isocyanate left after the reaction. This further supports the success of the modification reaction on ZIF-UC-6 and highlights that the reactive amine group is needed for the PSM reaction to occur.

CO_2 gas sorption on modified ZIF-UC-6 revealed a maximum CO_2 uptake of 43.3 cm^3 g^{-1} at STP (**Fig. S32, Table S9**), *i.e.*, an uptake very close to that observed for unmodified ZIF-UC-6 (46.9 cm^3 g^{-1} at STP). This suggests that PSM does not dramatically alter the porosity of the ZIF due to the low percentage conversion (*ca.* 1%) of the organic molecules within the framework. The modification reaction likely occurs mostly on the particle surface, *i.e.*, not affecting the internal pore structure of the ZIF. The slightly lower value for the maximum uptake of CO_2 in the modified material is attributed to the partial blocking of the pore network by the newly introduced alkyl chains from octyl isocyanate. The modified ZIF also exhibited more pronounced hysteresis compared to the unmodified material. This is also attributed to the newly introduced alkyl chains inhibiting the diffusion of CO_2 in the framework.

Modified ZIF-UC-6 was then examined using DSC and TGA (**Fig. S33-35**) to detect changes in its thermal behavior caused by PSM. Its thermal stability was identical to the unmodified material (**Fig. S33**). However, a mass loss (9.9%) between 200 °C and 346 °C (**Fig. S34**) may be attributed to partial decomposition of the modified linkers. The washing and activation procedure used here has been reported to remove most unreacted species.[33,47] Additionally, neat octyl isocyanate has a boiling point of 200-204 °C, *i.e.* lower than the observed mass loss here.[33] This mass loss was also accompanied by a sharp endo- and exothermic event in the DSC (**Fig. S35**). Desolvation is an endothermic process and occurs at lower temperatures than this event, which had a closer resemblance to thermal amorphization events in other ZIFs.[48,49] Interestingly, upon further heating, no indication of melting was detected. However, a possible T_g at 314 °C was observed upon reheating (**Fig. S35**) and subsequent PXRD confirmed the sample to be X-ray amorphous (**Fig. S36**). ^{1}H NMR spectroscopy revealed that, after heating, the carbon chains were still present in the structure to some extent, although the emergence of multiple new environments suggested partial decomposition had occurred (**Fig. S37**).

Preparation of Modified a_gZIF-UC-6 – Strategy (ii). As the above strategy resulted in significant sample decomposition, strategy (ii) *i.e.*, direct modification of a_gZIF-UC-6 was then attempted (**Methods**, **Fig. S38**). Briefly, a_gZIF-UC-6 was suspended in a dilute solution of octyl isocyanate in chloroform and left for 24 hr before the sample was washed and activated. CHN microanalysis on modified a_gZIF-UC-6 showed minimal differences when compared to the unmodified sample and this

is attributed again to the small fraction of the structure that undergoes the PSM reaction (**Table S10-S11**). ^{1}H NMR on the modified glass did not exhibit a peak in the imidazole region that corresponded to the modified linker (**Fig. S39b**). However, close inspection of the satellite peaks of the imidazole proton peak revealed asymmetric integration values suggesting that the modified linker in the glass could be masked by these peaks. This was accompanied by the presence of new aromatic linker environments of the expected intensity (**Fig. S39c**) and evidence of the carbon chain below 1.5 ppm (**Fig. S39d**). The composition of the modified glass was then determined and found to be identical to the crystalline sample $[Zn(Im)_{1.82}(abIm)_{0.16}(PSM\ linker)_{0.02}]$ *i.e.*, the same as strategy (i), an 11% conversion of the available abIm linkers and a 1% conversion of the total organic molecules present within the structure.

As with the crystalline sample, mass spectrometric analysis of modified a_gZIF-UC-6 showed the presence of the octyl-urea adduct, with formula $[C_{16}H_{24}N_4O]H^+$ (calc: *m/z* = 289.2028; found: *m/z* = 289.2023; 2.0 ppm) again confirming linker modification (**Figs. S40, S41**).

Modified a_gZIF-UC-6 displayed a maximum CO_2 uptake of 21.0 cm^3 g^{-1} at STP (**Fig. S42, Table S12**). This value was close to that observed for unmodified a_gZIF-UC-6 (23.0 cm^3 g^{-1} at STP). As for the crystalline sample, this indicates that the PSM procedure does not dramatically alter the porosity of the ZIF glass. The small difference in the uptake of CO_2 in the modified glass is again attributed to the presence of alkyl chains in the structure. The difference in maximum uptake between modified a_gZIF-UC-6 and modified ZIF-UC-6 is similar to the difference between their unmodified counterparts (**Fig. S43**), suggesting that the maximum CO_2 uptake is influenced more by the framework structure, *i.e.*, crystal or glass, than by the PSM process.

The thermal response of modified a_gZIF-UC-6 was investigated (**Fig. S44-46**) to identify changes in its thermal behavior caused by PSM. The thermal stability of the glass was largely unaffected by modification (**Fig. S44, S45**). However, a distinct change in the DSC of modified a_gZIF-UC-6 was observed (**Fig. S46**), with a broad T_g observed at 290 °C in the 1st upscan. This is different to the behavior of modified crystalline ZIF-UC-6 which exhibited a sharp endo- and exothermic event in the 1st upscan of the DSC. Upon re-heating modified a_gZIF-UC-6, a T_g was observed (319 °C), consistent with unmodified a_gZIF-UC-6. The behavior in the 1st upscan could be attributed to the partial decomposition of the modified linkers with heating. After thermal decomposition of these linkers, the bulk composition of the modified glass is likely to be very similar to the composition of the unmodified glass, resulting in a T_g more consistent with this material.

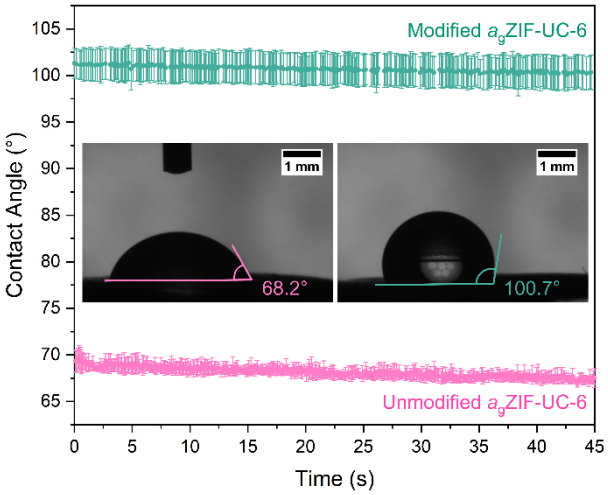

Figure 5. Water contact angle data collected on unmodified a_gZIF-UC-6 (pink) and modified a_gZIF-UC-6 (green) collected over 45 s. Insets: microscope images of water on the unmodified (left) and modified glass (right) surfaces showing overall mean contact angles of 68.2 ± 0.6° and 100.7 ± 2.2° respectively. Lines and angles drawn on these images are a guide only.

To demonstrate the ability of PSM to tune the bulk properties of the ZIF glass surface, two a_gZIF-UC-6 pellets were prepared. One was left unmodified, and the other was modified with octyl isocyanate in a similar manner to the glass powder described above (**Methods**). The hydrophobicity was then probed using water contact angle measurements (**Figs. 5, S47**). These measurements can only be performed on flat surfaces, making them ideal for studying the ZIF glass surface. (Hence an equivalent measurement of the modified crystalline ZIF-UC-6 powder was not possible.) The water contact angle measurements revealed that the unmodified glass surface was relatively hydrophilic with a mean water contact angle of 68.2 ± 0.6°. However, modification of the glass surface with carbon chains from octyl isocyanate caused a dramatic increase in the hydrophobicity of the glass surface, resulting in a mean water contact angle of 100.7 ± 2.2° (**Figs. 5, S47**). This clearly demonstrates the success of the modification reaction and highlights the promise of this method for tuning the properties of the ZIF glass surface.

To further demonstrate the scope of PSM for tuning the hydrophobicity of ZIF glasses, a third a_gZIF-UC-6 pellet was prepared before using an identical modification procedure — albeit this time with dodecyl isocyanate as the modification reagent (**Methods**). Hydrophobicity measurements revealed a water contact angle of 114.7 ± 2.7° (**Fig. S48**), *i.e.*, significantly higher than that observed after modification with octyl isocyanate. This implies that increasing carbon chain length results in an increase in hydrophobicity at the glass surface, although further experiments would be needed to confirm the veracity of this conclusion. Ultimately, it is hoped that the precise hydrophobicity of the ZIF glass surface could be controlled by judicious choice of the carbon chain length used during modification.

CONCLUSION

In this work we have successfully prepared a novel liquid and glass forming ZIF, denoted ZIF-UC-6. Crystallizing in the *Pbca* space group and exhibiting the **cag** topology, with composition $[Zn(Im)_{2-x}(abIm)_x]$ (where x = 0.18), the framework displays strong structural similarities with other glass forming ZIFs.[14] The amine functionality introduced into the framework by the abIm linker causes a lowering of both T_m (345 °C) and T_g (316 °C) compared to other **cag** topology ZIFs. Additionally, this amine functionality provided a promising target for PSM, thereby facilitating the modification of the ZIF in its crystalline form as well as the glass form for the first time.

As a prototypical example, we investigated the effect on the wetting ability of the glass surface by its reaction with octyl isocyanate. A 32.5° increase in the water contact angle after PSM supports the success of the reaction. Moreover, modification of the ZIF glass surface with dodecyl isocyanate resulted in an increase in the water contact angle by 46.5° compared to the un-

modified glass, implying that careful consideration of the carbon chain length can be used to precisely control the wetting behavior of the ZIF glass surface. These results confirm PSM as a promising strategy for tuning the hydrophobicity of the glass surface, almost independently of porosity. This enhancement in hydrophobicity could be utilized to facilitate the preparation of hydrophobic ZIF glass coatings for example. However, PSM of ZIF glasses is not limited to the reaction demonstrated here and, in fact, the library of PSM reactions that have been demonstrated in crystalline systems can now potentially be applied to glasses as well. Some potential avenues for future research could include surface modification to achieve catalytically active ZIF glasses, or the incorporation of photoresponsive functional groups to prepare light responsive ZIF glasses.[50] Further studies to expand PSM to other ZIF glasses, as well as incorporating additional chemical functionality at the glass surface are now underway.

METHODS

Materials. Imidazole (≥99.5%), D_2O (35 wt.% DCl), octyl isocyanate (97%), dodecyl isocyanate (99%) and chloroform (99.0-99.4% GC) were purchased from Sigma Aldrich. Dimethyl sulfoxide (DMSO)-d_6 (99.8 atom% D, contains 0.03% (v/v) tetramethylsilane (TMS)) was purchased from VWR. Zinc nitrate hexahydrate (98%) was purchased from Alfa Aesar. *N*,*N*-Dimethylformamide (DMF) (99.5%), chloroform (reagent grade) and dichloromethane stabilized with amylene (DCM) (99.8%) were purchased from Fischer Scientific. 5-Aminobenzimidazole (>99%) was purchased from Santa Cruz Biotechnology. All materials were used without further purification.

Single Crystal Synthesis of ZIF-UC-6. Zinc nitrate hexahydrate (0.095 g, 0.32 mmol), imidazole (0.460 g, 6.76 mmol) and 5-aminobenzimidazole (0.100 g, 0.75 mmol) were dissolved in DMF (4.7 mL) to give a dark red colored solution. This solution was heated to 130 °C and held there for 48 hr before being cooled to 30 °C at 5 °C hr^{-1}. The resulting burgundy crystals were collected by vacuum filtration, washed with fresh DMF, and stored in fresh DMF until needed.

Bulk Solvothermal Synthesis of ZIF-UC-6. Zinc nitrate hexahydrate (1.515 g, 5.09 mmol), imidazole (7.350 g, 108 mmol) and 5-aminobenzimidazole (1.598 g, 12.0 mmol) were dissolved in DMF (75 mL) to give a dark red colored solution. This solution was heated to 130 °C and held there for 48 hr in an oven before being removed and left to cool to room temperature naturally. The resulting burgundy polycrystalline powder was isolated by vacuum filtration and washed with fresh DMF. The sample was then soaked in DCM (5 mL) for 24 hr in a sealed vial to allow solvent exchange to take place. The powder was again isolated by vacuum filtration before being activated under vacuum at 170 °C for 3 hr. This synthetic method was designed based on the reported synthesis of ZIF-UC-5.[14]

Post-Synthetic Modification of ZIF-UC-6 and a_gZIF-UC-6 Powder. ZIF-UC-6 and a_gZIF-UC-6 (42 mg, 0.20 mmol, 0.04 mmol equivalents of -NH_2) were suspended in chloroform (2 mL). Octyl isocyanate (56 μL, 0.32 mmol, 8 equivalents compared to -NH_2) was added and the suspension was shaken to disperse the reagents. The suspension was left to stand for 24 hr. The powder was then collected by vacuum filtration and washed with chloroform (3 × 6 mL) before being soaked in fresh chloroform (3 mL) for a minimum of 3 days. The powder was again isolated by vacuum filtration before being activated under vacuum at 100 °C overnight (*ca.* 18 hr). This synthetic method was based on the PSM methods previously reported by Cohen *et al.* on IRMOF-3.[33,35] The exact same modification and washing procedure was performed for the control experiment using ZIF-62 (42 mg), where ZIF-62 was prepared using a previously reported method.[46]

Pellet Preparation of a_gZIF-UC-6. Crystalline ZIF-UC-6 (*ca.* 150 mg) was placed inside a 13 mm pellet die and compressed at a pressure of *ca.* 0.15 GPa for 1 min before the pressure was released. This gave a smooth pellet of crystalline ZIF-UC-6. This pellet was then melted by heating to 409 °C in a Carbolite tube furnace under a flowing argon atmosphere. After waiting for 1 min at 409 °C, the pelletized glass sample was cooled to 200 °C under flowing argon. The argon stream was then turned off and the sample was allowed to cool to room temperature. The loss of any defined Bragg reflections was then confirmed by PXRD.

Post-Synthetic Modification of a_gZIF-UC-6 Pellet – Octyl Isocyanate. A 13 mm a_gZIF-UC-6 pellet (66 mg, 0.31 mmol, 0.06 mmol equivalents of -NH_2) was suspended in chloroform (2 mL). Octyl isocyanate (85 μL, 0.48 mmol, 8 equivalents compared to -NH_2) was added and the suspension was left to stand for one day. The pellet was then collected by vacuum filtration and washed with chloroform (3 × 6 mL) before being soaked in fresh chloroform (3 mL) for 6 days. The pellet was again isolated by vacuum filtration before being activated under vacuum at 100 °C overnight (*ca.* 18 hr). This was based on the PSM methods previously reported on IRMOF-3.[33,35]

Post-Synthetic Modification of a_gZIF-UC-6 Pellet – Dodecyl Isocyanate. A 13 mm a_gZIF-UC-6 pellet (73 mg, 0.34 mmol, 0.07 mmol equivalents of -NH_2) was suspended in chloroform (2 mL). Dodecyl isocyanate (134 μL, 0.56 mmol, 8 equivalents compared to -NH_2) was added and the suspension was left to stand for one day. The pellet was then collected by vacuum filtration and washed according to the procedure described above.

Single Crystal X-ray Diffraction (SCXRD). Single crystal diffraction data were collected using a Brucker D8 VENTURE diffractometer equipped with a Brucker PHOTON II detector at 150 K using graphite monochromated Mo/Kα radiation (λ= 0.71073). Data reduction was done using the APEX3 program. Absorption correction based on multi-scan was obtained by SADABS. The structure was solved and refined using SHELXT and SHELXL packages correspondingly, using the OLEX2 program.[51–53] The electron density within the voids was accounted for using the SQUEEZE program implemented in PLATON.[54]

Crystal data for ZIF-UC-6: $C_{13.59}H_{12.78}N_{8.39}Zn_2$, M_r =424.36, crystal dimensions 0.195 × 0.156 × 0.077 mm, Orthorhombic, a =15.839(2) Å, b = 15.599(2) Å, c = 17.984(2) Å, $\alpha = \beta = \gamma = 90°$, V = 4443.3(9) $Å^3$, space group, *Pbca*, (No. 61), T = 150 K, Z = 8, 24514 measured reflections, 4524 independent reflections (R_{int} = 0.0593), which were used in all calculations. The final R_1 = 0.053 for 3285 observed data $R[F^2 > 2\sigma(F^2)]$ and $wR(F^2)$ = 0.139 (all data). CSD deposition 2115059.

Powder X-ray Diffraction (PXRD). Data were collected on a Bruker D8 ADVANCE diffractometer equipped with a position sensitive LynxEye detector with Bragg-Brentano parafocusing geometry. Cu Kα (λ = 1.5418 Å) radiation was used. The samples were compacted into 5 mm disks on a low background silicon substrate and rotated during data collection in the 2θ range of 5–40° at ambient temperature. All data conversion from .raw files to .xy files was performed using PowDLL.[55] Pawley refinements were performed using TOPAS-Academic

Version 6.[56] Thompson-Cox-Hastings pseudo-Voigt (TCHZ) peaks shapes were used along with a simple axial divergence correction. The lattice parameters were refined in the 2θ range of 5–40° against the values obtained from the CIF for ZIF-UC-6 reported in this work. The zero-point error was also refined.

Differential Scanning Calorimetry (DSC). Data were collected on a Netzsch DSC 214 Polyma Instrument. Heating and cooling rates of 10 °C min^{-1} were used in conjunction with a flowing argon atmosphere. Sealed aluminium pans (30 μL) were used with a hole punctured in the lid to prevent pressure build-up. An empty aluminium pan was used as a reference. Background corrections were performed using the same heating cycle on an empty aluminium crucible. All data analysis was performed using the Netzsch *Proteus*® software package. T_m was taken as the offset (the end point) of the melting endotherm. T_g was taken as the mid-point of the change in gradient of the heat flow of the DSC on the 2nd upscan.

Thermogravimetric Analysis (TGA). Data were collected on a TA Instruments SDT-Q600 using alumina pans (90 μL). Heating and cooling rates of 10 °C min^{-1} were used, and experiments were conducted under a flowing argon atmosphere. All data analysis was performed using the TA Instruments Universal Analysis software package. The temperature used to define any weight changes was determined using the first derivative of the weight (%) trace as a function of temperature.

^{1}H Nuclear Magnetic Resonance (NMR) Spectroscopy. ^{1}H NMR spectra were recorded at 298 K using a Bruker AVIII 500 MHz Spectrometer with a dual ^{13}C/^{1}H (DCH) cryoprobe at the Department of Chemistry, University of Cambridge. Samples of crystalline ZIF-UC-6 and a_gZIF-UC-6 were dissolved in a mixture of DCl (35%)/D_2O and DMSO-d_6 in a 1:5 ratio with tetramethylsilane (TMS) used as a reference. For samples of ZIF-UC-6 and a_gZIF-UC-6 which had undergone PSM, as well as unreacted imidazole and 5-aminobenzimidazole, *ca.* 5.5 mg of sample was dissolved in DMSO-d_6 (1.5 mL) and a dilute solution of DCl (200 μL) with TMS again used as a reference. This dilute solution was prepared from DCl (35%)/D_2O (23 μL) and DMSO-d_6 (1 mL). Dilute conditions were used to prevent acid catalyzed hydrolysis of the newly formed urea functionalized linkers. These conditions were based on those used by Cohen *et al.* in their studies on PSM of IRMOF-3.[33] ^{1}H NMR spectra were also collected on octyl isocyanate (dissolved in DMSO-d_6 only to prevent any reaction with DCl/D_2O). The sample of ZIF-62 used as PSM control was dissolved in a mixture of DCl (35%)/D_2O and DMSO-d_6 in a 1:5 ratio with tetramethylsilane (TMS) as a reference. All data processing was performed using the Bruker TopSpin 4.0.7 software package.

Mass Spectrometry. High resolution electrospray ionization mass spectra were collected on an Agilent 6546 QTOF-MS in positive ion mode using direct infusion. Samples of modified ZIF-UC-6 and a_gZIF-UC-6 were suspended in an aqueous Na_2EDTA solution (0.6 M), HCl added dropwise until solids had dissolved, and extracted with $CHCl_3$. The organic layer was then dried over Na_2SO_4 and evaporated, before dissolution in methanol prior to injection, and run in 70:30 *v*/*v* MeCN:H_2O with 1% formic acid. This methodology is adapted from previously reported protocols for analysis of MOF surface modification.[57]

CO_2 Gas Sorption: Measurements were performed on a Micromeritics ASAP 2020 surface area and porosity analyzer. Samples of ZIF-UC-6 (*ca.* 140 mg), a_gZIF-UC-6 (*ca.* 110 mg), modified ZIF-UC-6 (*ca.* 60 mg) and modified a_gZIF-UC-6 (*ca.* 90 mg) were degassed by heating under vacuum at 100 °C for 12 hr before analysis using carbon dioxide gas at 273 K. Gas uptake was determined using the Micromeritics MicroActive software package.

Diffuse-Reflectance UV-Vis Spectroscopy (DRUV). Measurements were carried out using a PerkinElmer Lambda 750 spectrophotometer equipped with a Labsphere 60 mm RSA ASSY integrating sphere. Samples were measured in a powder sample holder with a fused quartz disc. Spectra were then transformed using the Kubelka-Munk transformation.[58,59]

Fourier-Transform Infrared (FTIR) Spectroscopy. IR spectra were collected on powder samples using a Bruker Tensor 27 FTIR spectrometer in transmission mode between 550 and 4000 cm^{-1}. A background was subtracted from all spectra prior to analysis.

Scanning Electron Microscopy (SEM). SEM images were collected with a high-resolution scanning electron microscope FEI Nova Nano SEM 450, accelerating voltage 15 kV. All samples were prepared by dispersing the material onto double sided adhesive conductive carbon tape that was attached to a flat aluminium sample holder and coated with a platinum layer of 15 nm.

CHN Microanalysis. CHN combustion analysis experiments were performed using a CE440 Elemental Analyzer, EAI Exeter Analytical Inc. ~1.3-1.5 mg of sample was used for each run. Measurements were collected up to 3 times per sample.

X-ray Total Scattering – Pair Distribution Function (PDF). X-ray total scattering data were collected at beamline I15-1, Diamond Light Source, UK (EE20038) on crystalline ZIF-UC-6 and glass a_gZIF-UC-6. A bulk sample of a_gZIF-UC-6 was prepared by heating crystalline ZIF-UC-6 (100 mg) to 400 °C (and holding it there for 1 min before cooling) in a Carbolite tube furnace under a flowing argon atmosphere. Both samples were ground and loaded into borosilicate glass capillaries (1.17 mm inner diameter) to heights of 3.7 cm (ZIF-UC-6) and 3.8 cm (a_gZIF-UC-6). The capillaries were then sealed before being mounted onto the beamline. Total scattering data were collected at room temperature for the background (*i.e.*, empty instrument), empty borosilicate capillary and for both samples in a Q range of 0.4 – 26.0 $Å^{-1}$ (λ = 0.161669 Å, 76.69 keV). Data for a_gZIF-UC-6 were collected at 100% flux. Data for crystalline ZIF-UC-6 were collected at 10% flux to prevent saturation of the detector due to the high crystallinity of this sample. The total scattering data were processed to account for the difference in beam flux incident on each sample, along with absorption corrections and various scattering corrections – background scattering, multiple scattering, container scattering and Compton scattering – in a Q range of 0.55–26.0 $Å^{-1}$. The crystallographic density of ZIF-UC-6 was taken as the density for both ZIF-UC-6 and a_gZIF-UC-6 during the data processing. Subsequent Fourier transformation of the processed total scattering data resulted in a real space pair distribution function $G(r)$ for each material. In this work, we use the $D(r)$ form of the pair distribution function to accentuate high r correlations. All processing of the total scattering data was performed using GudrunX following well documented procedures.[60–62]

Contact Angle Measurements. An FTA1000 B class instrument was used to acquire contact angles between water and the surface of modified and unmodified a_gZIF-UC-6 pellets (13 mm diameter). Static contact angles of a droplet of water (*ca.* 10 μL) were measured over a period of 45 s and an average of at least 3 droplets was taken for each sample. All analysis

was performed using the FTA32 software package.[63] The overall mean contact angle for each surface was then determined.

ASSOCIATED CONTENT

Supporting Information. The supporting information for this works is available free of charge on the ACS publication website. Detailed experimental methods and techniques, synthesis and characterization of ZIF-UC-6, a_gZIF-UC-6 and modified samples including optical microscopy, SCXRD, PXRD, DRUV, CO_2 gas sorption, ^{1}H NMR, TGA, DSC, SEM, X-ray total scattering, FTIR, CHN microanalysis and water contact angle measurements.

AUTHOR INFORMATION

Corresponding Author

Thomas D. Bennett − *Department of Materials Science and Metallurgy, University of Cambridge, Cambridge CB3 0FS, United Kingdom*; https://orcid.org/0000-0003-3717-3119; Email: tdb35@cam.ac.uk

Authors

Alice M. Bumstead − *Department of Materials Science and Metallurgy, University of Cambridge, Cambridge CB3 0FS, United Kingdom;* https://orcid.org/0000-0001-9269-1731
Ignas Pakamorė − *WestCHEM, School of Chemistry, The University of Glasgow, University Avenue, Glasgow, G12 8QQ, United Kingdom.*
Kieran D. Richards − *Department of Materials Science and Metallurgy, University of Cambridge, Cambridge CB3 0FS, United Kingdom;* https://orcid.org/0000-0001-8968-3730
Michael F. Thorne − *Department of Materials Science and Metallurgy, University of Cambridge, Cambridge CB3 0FS, United Kingdom;* https://orcid.org/0000-0002-3188-2478
Sophia S. Boyadjieva − *WestCHEM, School of Chemistry, The University of Glasgow, University Avenue, Glasgow, G12 8QQ, United Kingdom.*
Celia Castillo-Blas – *Department of Materials Science and Metallurgy, University of Cambridge, Cambridge CB3 0FS, United Kingdom*; https://orcid.org/0000-0002-9481-5395
Lauren N. McHugh − *Department of Materials Science and Metallurgy, University of Cambridge, Cambridge CB3 0FS, United Kingdom;* https://orcid.org/0000-0003-2032-0450
Adam F. Sapnik − *Department of Materials Science and Metallurgy, University of Cambridge, Cambridge CB3 0FS, United Kingdom;* https://orcid.org/0000-0001-6200-4208
Dean S. Keeble − *Diamond Light Source Ltd, Diamond House, Harwell Campus, Didcot, Oxfordshire, OX11 0DE, United Kingdom;* https://orcid.org/0000-0003-4225-3770
David A. Keen − *ISIS Facility, Rutherford Appleton Laboratory, Harwell Campus, Didcot, Oxfordshire, OX11 0QX, United Kingdom;* https://orcid.org/0000-0003-0376-2767
Rachel C. Evans − *Department of Materials Science and Metallurgy, University of Cambridge, Cambridge CB3 0FS, United Kingdom;* https://orcid.org/0000-0003-2956-4857
Ross S. Forgan − *WestCHEM, School of Chemistry, The University of Glasgow, University Avenue, Glasgow, G12 8QQ, United Kingdom;* https://orcid.org/0000-0003-4767-6852

Author Contributions

All authors have given approval to the final version of the manuscript.

Notes

The authors declare no competing financial interest.

ACKNOWLEDGMENTS

A.M.B. acknowledges the Royal Society for funding (RGF\EA\180092) as well as the Cambridge Trust for a Vice Chancellor's Award (304253100). M.F.T. would like to thank Corning Incorporated for PhD funding. A.F.S. acknowledges the EPSRC for a PhD studentship under the industrial CASE scheme along with Johnson Matthey PLC (JM11106). K.D.R. acknowledges the EPSRC (EP/R513180/1) for a PhD studentship. T.D.B. thanks the Royal Society for both a University Research Fellowship (UF150021) and a research grant (RSG\R1\180395) as well as the University of Canterbury Te Whare Wānanga o Waitaha, New Zealand, for a University of Cambridge Visiting Canterbury Fellowship. T.D.B. and L.N.M. also thank the Leverhulme Trust for a Philip Leverhulme Prize. T.D.B. and C.C.B. also gratefully acknowledge funding by a Leverhulme Trust Research Project Grant (RPG-2020-005). R.S.F. thanks the Royal Society for a University Research Fellowship (UF110655 / UF160394) and the University of Glasgow for funding. We extend our gratitude to Diamond Light Source, Rutherford Appleton Laboratory, U.K., for the provision of synchrotron access to Beamline I15-1 (EE20038) and thank Thomas Forrest for his assistance with data collection. We also extend out thanks to Andrew Mason and Duncan Howe for collection of all liquid state ^{1}H NMR spectroscopy data and to Nigel Howard for performing CHN microanalysis, all at the Yusuf Hamied Department of Chemistry, University of Cambridge. We would also like to thank Dr Bikash Kumar Shaw for valuable discussions.

REFERENCES

(1) Horike, S.; Shimomura, S.; Kitagawa, S. Soft Porous Crystals. *Nat. Chem.* **2009**, *1* (9), 695–704.
(2) Schneemann, A.; Bon, V.; Schwedler, I.; Senkovska, I.; Kaskel, S.; Fischer, R. A. Flexible Metal-Organic Frameworks. *Chem. Soc. Rev.* **2014**, *43* (16), 6062–6096.
(3) Coudert, F. X. Responsive Metal-Organic Frameworks and Framework Materials: Under Pressure, Taking the Heat, in the Spotlight, with Friends. *Chem. Mater.* **2015**, *27* (6), 1905–1916.
(4) Bennett, T. D.; Cheetham, A. K.; Fuchs, A. H.; Coudert, F. X. Interplay between Defects, Disorder and Flexibility in Metal-Organic Frameworks. *Nat. Chem.* **2016**, *9* (1), 11–16.
(5) Horike, S.; Nagarkar, S. S.; Ogawa, T.; Kitagawa, S. A New Dimension for Coordination Polymers and Metal–Organic Frameworks: Towards Functional Glasses and Liquids. *Angew. Chemie - Int. Ed.* **2019**, 2–15.
(6) Gaillac, R.; Pullumbi, P.; Beyer, K. A.; Chapman, K.; Keen, D. A.; Bennett, T. D.; Coudert, F. X. Liquid Metal–Organic Frameworks. *Nat. Mater.* **2017**, *16*, 1149–1154.
(7) Bennett, T. D.; Horike, S. Liquid, Glass and Amorphous Solid States of Coordination Polymers and Metal–Organic Frameworks. *Nat. Rev. Mater.* **2018**, *3*, 431–440.
(8) Park, K. S.; Ni, Z.; Cote, A. P.; Choi, J. Y.; Huang, R.; Uribe-Romo, F. J.; Chae, H. K.; O'Keeffe, M.; Yaghi, O. M. Exceptional Chemical and Thermal Stability of Zeolitic Imidazolate Frameworks. *Proc. Natl. Acad. Sci.* **2006**, *103* (27), 10186–10191.
(9) Zhang, J. P.; Zhang, Y. B.; Lin, J. Bin; Chen, X. M. Metal Azolate Frameworks: From Crystal Engineering to Functional Materials. *Chem. Rev.* **2012**, *112* (2), 1001–1033.
(10) Bumstead, A. M.; Thorne, M. F.; Bennett, T. D. Identifying the Liquid and Glassy States of Coordination Polymers and Metal–Organic Frameworks. *Faraday Discuss.* **2021**, *225*, 210–225.
(11) Frentzel-Beyme, L.; Kloß, M.; Pallach, R.; Salamon, S.; Moldenhauer, H.; Landers, J.; Wende, H.; Debus, J.; Henke, S. Porous Purple Glass – A Cobalt Imidazolate Glass with Accessible Porosity from a Meltable Cobalt Imidazolate Framework. *J. Mater. Chem. A* **2019**, *7* (3), 985–990.
(12) Frentzel-Beyme, L.; Kloß, M.; Kolodzeiski, P.; Pallach, R.; Henke, S. Meltable Mixed-Linker Zeolitic Imidazolate Frameworks and Their Microporous Glasses - From Melting Point Engineering to Selective Hydrocarbon Sorption. *J. Am.*

Chem. Soc. **2019**, *141*, 12362–12371.
(13) Thorne, M. F.; Rios Gomez, M. L.; Bumstead, A. M.; Li, S.; Bennett, T. D. Mechanochemical Synthesis of Mixed Metal, Mixed Linker Glass-Forming Metal–Organic Frameworks. *Green Chem.* **2020**, *22* (8), 2505–2512.
(14) Bumstead, A. M.; Rios Gomez, M. L.; Thorne, M. F.; Sapnik, A. F.; Longley, L.; Tuffnell, J. M.; Keeble, D. S.; Keen, D. A.; Bennett, T. D. Investigating the Melting Behaviour of Polymorphic Zeolitic Imidazolate Frameworks. *CrystEngComm* **2020**, *22*, 3627–3637.
(15) Hou, J.; Ríos Gómez, M. L.; Krajnc, A.; McCaul, A.; Li, S.; Bumstead, A. M.; Sapnik, A. F.; Deng, Z.; Lin, R.; Chater, P. A.; Keeble, D. S.; Keen, D. A.; Appadoo, D.; Chan, B.; Chen, V.; Mali, G.; Bennett, T. D. Halogenated Metal–Organic Framework Glasses and Liquids. *J. Am. Chem. Soc.* **2020**, *142* (8), 3880–3890.
(16) Morris, W.; Leung, B.; Furukawa, H.; Yaghi, O. K.; He, N.; Hayashi, H.; Houndonougbo, Y.; Asta, M.; Laird, B. B.; Yaghi, O. M. A Combined Experimental-Computational Investigation of Carbon Dioxide Capture in a Series of Isoreticular Zeolitic Imidazolate Frameworks. *J. Am. Chem. Soc.* **2010**, *132* (32), 11006–11008.
(17) Cho, K. Y.; An, H.; Do, X. H.; Choi, K.; Yoon, H. G.; Jeong, H. K.; Lee, J. S.; Baek, K. Y. Synthesis of Amine-Functionalized ZIF-8 with 3-Amino-1,2,4-Triazole by Postsynthetic Modification for Efficient CO2-Selective Adsorbents and Beyond. *J. Mater. Chem. A* **2018**, *6* (39), 18912–18919.
(18) Gelles, T.; Lawson, S.; Rownaghi, A. A.; Rezaei, F. Recent Advances in Development of Amine Functionalized Adsorbents for CO2 Capture. *Adsorption* **2020**, *26*, 5–50.
(19) Cohen, S. M. Postsynthetic Methods for the Functionalization of Metal-Organic Frameworks. *Chem. Rev.* **2012**, *112* (2), 970–1000.
(20) Marshall, R. J.; Forgan, R. S. Postsynthetic Modification of Zirconium Metal-Organic Frameworks. *Eur. J. Inorg. Chem.* **2016**, 4310–4331.
(21) Burrows, A. D. Mixed-Component Metal-Organic Frameworks (MC-MOFs): Enhancing Functionality through Solid Solution Formation and Surface Modifications. *CrystEngComm* **2011**, *13* (11), 3623–3642.
(22) Lin, Y.; Zhang, Q.; Zhao, C.; Li, H.; Kong, C.; Shen, C.; Chen, L. An Exceptionally Stable Functionalized Metal-Organic Framework for Lithium Storage. *Chem. Commun.* **2015**, *51* (4), 697–699.
(23) Xiang, L.; Sheng, L.; Wang, C.; Zhang, L.; Pan, Y.; Li, Y. Amino-Functionalized ZIF-7 Nanocrystals: Improved Intrinsic Separation Ability and Interfacial Compatibility in Mixed-Matrix Membranes for CO2/CH4 Separation. *Adv. Mater.* **2017**, *29* (32), 1–8.
(24) Fonseca, J.; Gong, T.; Jiao, L.; Jiang, H.-L. Metal-Organic Frameworks (MOFs) beyond Crystallinity: Amorphous MOFs, MOF Liquids and MOF Glasses. *J. Mater. Chem. A* **2021**, 10562–10611.
(25) Gy, R. Ion Exchange for Glass Strengthening. *Mater. Sci. Eng. B* **2008**, *149*, 159–165.
(26) The Secret of Tough Glass: Ion Exchange https://www.corning.com/emea/en/innovation/the-glass-age/science-of-glass/the-secret-of-tough-glass-ion-exchange.html (accessed 2021-05-21).
(27) Arnold, G. W. Ion Implantation Effects in Glasses. *Radiat. Eff.* **1982**, *65*, 17–30.
(28) Magruder, R. H.; Zuhr, R. A.; Osborne, D. H. Modification of the Optical Properties of Glass by Sequential Ion Implantation. *Nucl. Instruments Methods Phys. Res. B* **1995**, *99*, 590–593.
(29) Múgica-Vidal, R.; Alba-Elías, F.; Sainz-García, E.; Ordieres-Meré, J. Atmospheric Plasma-Polymerization of Hydrophobic and Wear-Resistant Coatings on Glass Substrates. *Surf. Coat. Technol.* **2014**, *259*, 374–385.
(30) Kim, H. M.; Sohn, S.; Ahn, J. S. Transparent and Super-Hydrophobic Properties of PTFE Films Coated on Glass Substrate Using RF-Magnetron Sputtering and Cat-CVD Methods. *Surf. Coat. Technol.* **2013**, *228*, 389–392.
(31) Levitz, P.; Ehret, G.; Sinha, S. K.; Drake, J. M. Porous Vycor Glass: The Microstructure as Probed by Electron Microscopy, Direct Energy Transfer, Small-angle Scattering, and Molecular Adsorption. *J. Chem. Phys.* **1991**, *95* (8), 6151–6161.
(32) Hood, H. P.; Nordberg, M. E. Method of Treating Borosilicate Glasses. US2286275A, 1940.
(33) Wang, Z.; Cohen, S. M. Postsynthetic Covalent Modification of a Neutral Metal-Organic Framework. *J. Am. Chem. Soc.* **2007**, *129* (41), 12368–12369.
(34) Kandiah, M.; Usseglio, S.; Svelle, S.; Olsbye, U.; Lillerud, K. P.; Tilset, M. Post-Synthetic Modification of the Metal-Organic Framework Compound UiO-66. *J. Mater. Chem.* **2010**, *20* (44), 9848–9851.
(35) Dugan, E.; Wang, Z.; Okamura, M.; Medina, A.; Cohen, S. M. Covalent Modification of a Metal-Organic Framework with Isocyanates: Probing Substrate Scope and Reactivity. *Chem. Commun.* **2008**, *7345* (29), 3366–3368.
(36) Costa, J. S.; Gamez, P.; Black, C. A.; Roubeau, O.; Teat, S. J.; Reedijk, J. Chemical Modification of a Bridging Ligand inside a Metal-Organic Framework While Maintaining the 3D Structure. *Eur. J. Inorg. Chem.* **2008**, 1551–1554.
(37) Banerjee, R.; Phan, A.; Wang, B.; Knobler, C.; Furukawa, H.; O'Keeffe, M.; Yaghi, O. M. High-Throughput Synthesis of Zeolitic Imidazolate Frameworks and Application to CO2 Capture. *Science* **2008**, *319* (5865), 939–943.
(38) Liu, M.; McGillicuddy, R. D.; Vuong, H.; Tao, S.; Slavney, A. H.; Gonzalez, M. I.; Billinge, S. J. L.; Mason, J. A. Network-Forming Liquids from Metal-Bis(Acetamide) Frameworks with Low Melting Temperatures. *J. Am. Chem. Soc.* **2021**, *143* (7), 2801–2811.
(39) Bondi, A. Van Der Waals Volumes and Radii. *J. Phys. Chem.* **1964**, *68* (3), 441–451.
(40) Yang, J.; Zhang, Y. B.; Liu, Q.; Trickett, C. A.; Gutiérrez-Puebla, E.; Monge, M. Á.; Cong, H.; Aldossary, A.; Deng, H.; Yaghi, O. M. Principles of Designing Extra-Large Pore Openings and Cages in Zeolitic Imidazolate Frameworks. *J. Am. Chem. Soc.* **2017**, *139* (18), 6448–6455.
(41) Debenedetti, P. G.; Stillinger, F. H. Supercooled Liquids and the Glass Transition. *Nature* **2001**, *410*, 259–267.
(42) Phan, A.; Doonan, C. J.; Uribe-romo, F. J.; Knobler, C. B.; Keeffe, M. O.; Yaghi, O. M. Capture Properties of Zeolitic Imidazolate Frameworks. *Acc. Chem. Res.* **2010**, *43* (1), 58–67.
(43) Cohen, S. M. The Postsynthetic Renaissance in Porous Solids. *J. Am. Chem. Soc.* **2017**, *139* (8), 2855–2863.
(44) Howarth, A. J.; Liu, Y.; Li, P.; Li, Z.; Wang, T. C.; Hupp, J. T.; Farha, O. K. Chemical, Thermal and Mechanical Stabilities of Metal-Organic Frameworks. *Nat. Rev. Mater.* **2016**, *1* (15018), 1–15.
(45) McGuire, C. V.; Forgan, R. S. The Surface Chemistry of Metal-Organic Frameworks. *Chem. Commun.* **2015**, *51* (25), 5199–5217.
(46) Widmer, R. N.; Lampronti, G. I.; Anzellini, S.; Gaillac, R.; Farsang, S.; Zhou, C.; Belenguer, A. M.; Wilson, C. W.; Palmer, H.; Kleppe, A. K.; Wharmby, M. T.; Yu, X.; Cohen, S. M.; Telfer, S. G.; Redfern, S. A. T.; Coudert, F.-X.; MacLeod, S. G.; Bennett, T. D. Pressure Promoted Low-Temperature Melting of Metal–Organic Frameworks. *Nat. Mater.* **2019**, *18*, 370–376.
(47) Rowsell, J. L. C.; Yaghi, O. M. Effects of Functionalization, Catenation, and Variation of the Metal Oxide and Organic Linking Units on the Low-Pressure Hydrogen Adsorption Properties of Metal-Organic Frameworks. *J. Am. Chem. Soc.* **2006**, *128* (4), 1304–1315.
(48) Bennett, T. D.; Keen, D. A.; Tan, J. C.; Barney, E. R.; Goodwin, A. L.; Cheetham, A. K. Thermal Amorphization of Zeolitic Imidazolate Frameworks. *Angew. Chem. Int. Ed.* **2011**, *50* (13), 3067–3071.
(49) Bennett, T. D.; Tan, J. C.; Yue, Y.; Baxter, E.; Ducati, C.; Terrill, N. J.; Yeung, H. H. M.; Zhou, Z.; Chen, W.; Henke, S.; Cheetham, A. K.; Greaves, G. N. Hybrid Glasses from Strong and Fragile Metal-Organic Framework Liquids. *Nat. Commun.* **2015**, *6* (8079), 1–7.
(50) Yin, Z.; Wan, S.; Yang, J.; Kurmoo, M.; Zeng, M. H. Recent Advances in Post-Synthetic Modification of Metal–Organic Frameworks: New Types and Tandem Reactions. *Coord. Chem. Rev.* **2019**, *378*, 500–512.
(51) Sheldrick, G. M. SHELXT - Integrated Space-Group and Crystal-Structure Determination. *Acta Crystallogr.* **2015**, *A71*, 3–8.
(52) Sheldrick, G. M. Crystal Structure Refinement with SHELXL.

Acta Crystallogr. **2015**, *C71*, 3–8.
(53) Dolomanov, O. V.; Bourhis, L. J.; Gildea, R. J.; Howard, J. A. K.; Puschmann, H. OLEX2: A Complete Structure Solution, Refinement and Analysis Program. *J. Appl. Crystallogr.* **2009**, *42* (2), 339–341.
(54) Spek, A. L. Structure Validation in Chemical Crystallography. *Acta Crystallogr. Sect. D Biol. Crystallogr.* **2009**, *65* (2), 148–155.
(55) Kourkoumelis, N. PowDLL, a Reusable .NET Component for Interconverting Powder Diffraction Data: Recent Developments. In *ICDD Annual Spring Meetings*; O'Neill, L., Ed.; Cambridge University Press: Powder Diffraction, 2013; Vol. 28, pp 137–148.
(56) Coelho, A. A. TOPAS and TOPAS-Academic: An Optimization Program Integrating Computer Algebra and Crystallographic Objects Written in C++. *J. Appl. Crystallogr.* **2018**, *51* (1), 210–218.
(57) Abánades Lázaro, I.; Haddad, S.; Sacca, S.; Orellana-Tavra, C.; Fairen-Jimenez, D.; Forgan, R. S. Selective Surface PEGylation of UiO-66 Nanoparticles for Enhanced Stability, Cell Uptake, and PH-Responsive Drug Delivery. *Chem* **2017**, *2* (4), 561–578.
(58) Kubelka, P.; Munk, F. An Article on Optics of Paint Layers. *Z. Tech. Phys.* **1931**, *12*, 593–601.
(59) Kubelka, P. New Contributions to the Optics of Intensely Light-Scattering Materials. *J. Opt. Soc. Am.* **1948**, *38* (5), 448–457.
(60) Soper, A. K.; Barney, E. R. Extracting the Pair Distribution Function from White-Beam X-Ray Total Scattering Data. *J. Appl. Crystallogr.* **2011**, *44* (4), 714–726.
(61) Soper, A. K. *GudrunN and GudrunX: Programs for Correcting Raw Neutron and X-Ray Diffraction Data to Differential Scattering Cross Section*; Technical Report RAL-TR-2011-013; Science and Technology Facilities Council, 2011. https://epubs.stfc.ac.uk/manifestation/6710/RAL-TR-2011-013.pdf (accessed 2021-09-24).
(62) Keen, D. A. A Comparison of Various Commonly Used Correlation Functions for Describing Total Scattering. *J. Appl. Crystallogr.* **2001**, *34* (2), 172–177.
(63) Woodward, R. *Fta32 Version 2.1*; First Ten Angstroms, Inc.: Newark 2015. https://www.firsttenangstroms.com/copy-of-additional-product-info-she (accessed 2021-09-24).

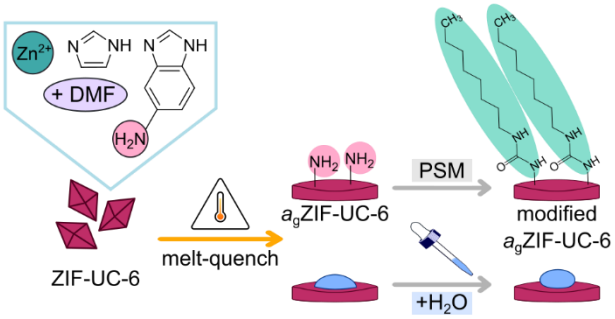

Table of Contents Figure